HHS Public Access

Author manuscript

Mol Cancer Res. Author manuscript; available in PMC 2024 January 05.

Published in final edited form as:

Mol Cancer Res. 2023 July 05; 21(7): 698–712. doi:10.1158/1541-7786.MCR-23-0003.

BZW2 inhibition reduces colorectal cancer growth and metastasis

Sumit Agarwal[1], **Farrukh Afaq**[1], **Prachi Bajpai**[1], **Michael Behring**[1], **Hyung-Gyoon Kim**[1], **Amith Varambally**[2], **Darshan S. Chandrashekar**[1], **Shajan Peter**[3,6], **Sameer Al Diffalha**[1,6], **Moh'd Khushman**[4], **Andreas Seeber**[5], **Sooryanarayana Varambally**[1,6], **Upender Manne, M.S., Ph.D.**[1,6,*]

[1]Department of Pathology, University of Alabama at Birmingham, Birmingham, AL

[2]Vestavia Hills High School, Vestavia Hills, AL

[3]Department of Medicine, Division of Gastroenterology, University of Alabama at Birmingham, Birmingham, AL

[4]Department of Medicine, Division of Hematology and Oncology, Washington University, St. Louis, MO

[5]Department of Hematology and Oncology, Comprehensive Cancer Center Innsbruck, Medical University of Innsbruck, Innsbruck, Austria

[6]Comprehensive Cancer Center, University of Alabama at Birmingham, Birmingham, AL

Abstract

Since survival of metastatic colorectal cancer (CRC) patients remain poor, there is an urgent need to identify potential novel druggable targets that are associated with CRC progression. One such target, basic leucine zipper and W2 domains 2 (BZW2), is involved in regulation of protein translation, and its overexpression is associated with human malignancy. Thus, we investigated the expression and regulation of BZW2, assessed its role in activation of WNT/β-catenin signaling, identified its downstream molecules, and demonstrated its involvement in metastasis of CRC. In human CRCs, high mRNA and protein expression levels of BZW2 were associated with tumor progression. BZW2-knockdown reduced malignant phenotypes, including cell proliferation, invasion, and spheroid and colony formation. BZW2-knockdown also reduced tumor growth and

[*]**Corresponding Author:** Upender Manne, M.S., Ph.D., Professor of Pathology, Division of Anatomic Pathology, Department of Pathology, Room # 20A, 4th Floor, Wallace Tumor Institute, University of Alabama at Birmingham, Birmingham, AL 35233, USA, upendermanne@uabmc.edu; Phone: (205) 934 4276.

Author Contributions

S. Agarwal: Conceptualization, laboratory investigations, methodology, data curation, formal analysis, and writing–original draft. **F. Afaq:** Laboratory investigations, data curations, formal analysis, writing -original draft. **P. Bajpai:** Laboratory investigations data curation, formal analysis, and writing–original draft. **M. Behring:** Bioinformatic and statistical analysis. **H-G. Kim:** Animal investigations. **A. Varambally:** Data acquisition and analyses. **D. S. Chandrashekar:** Bioinformatic analysis. **S. P. Sugandha:** Resources. **S. Al Diffalha:** Analyzed histopathology and IHC evaluations. **Moh'd. Khushman:** Investigations and resources. **A. Seeber:** Experimental consultations. **S. Varambally:** Conceptualization, resources, manuscript draft preparation and editing. **U. Manne:** Conceptualization, methodology, resources, funding acquisition, project administration, writing and editing.

Conflict of interest: The authors declare no conflict of interest.

Supplementary Information: Supplementary material that is directly relevant to the studies reported in the article are included separately.

metastasis; conversely, transfection of BZW2 into BZW2 low-expressing CRC cells promoted malignant features, including tumor growth and metastasis. BZW2 expression was coordinately regulated by microRNA-98, c-Myc, and histone methyltransferase EZH2. RNA sequencing analyses of CRC cells modulated for BZW2 identified P4HA1 and the long non-coding RNAs, MALAT1 and NEAT1, as its downstream targets. Further, BZW2 activated the Wnt/β-catenin signaling pathway in CRCs expressing wild-type β-catenin. In sum, our study suggests the possibility of targeting BZW2 expression by inhibiting EZH2 and/or c-Myc.

Keywords

Colorectal cancer; BZW2; WNT/β-catenin signaling; EZH2; metastasis

Introduction

Worldwide, colorectal cancer (CRC), a molecularly heterogeneous disease, is a leading cause of cancer-related deaths (1). Despite advances in therapeutic modalities, the overall survival rate for metastatic CRC remains poor. Thus, there is a need to identify new therapeutic molecular targets to improve CRC patient survival.

Basic leucine zipper and W2 domains 2 (BZW2), also known as translation initiation regulator eIF5-mimic protein 1 (5MP1), is a member of the basic-region leucine zipper (bZIP) superfamily of transcription factors. BZW2 has partial homology with eIF5 and can function as a competitive inhibitor of eIF5 (2). Studies have shown that BZW2 is an oncogene that is involved in progression of various types of cancers (3–7). In osteosarcomas, BZW2 is upregulated via activation of the Akt/mTOR signaling pathway, and its knockdown arrests osteosarcoma cells at the G2/M phase (3). BZW2 is also upregulated in hepatocellular carcinomas, and its silencing decreases cell malignant phenotypes (4). In muscle-invasive bladder cancers, silencing of BZW2 -inhibits cell growth and -induces G1 arrest and apoptosis (5), suggesting that BZW2 functions in tumor -progression. In CRCs, BZW2 is overexpressed relative to healthy tissue, and it is involved in the growth of CRC cells (6, 7) *via* activating ERK/MAPK signaling (6). Furthermore, c-Myc is a target of translation reprogramming by BZW2 (7).

In the present study, we described the regulation of BZW2 overexpression and identified its downstream targets, its role in metastasis, and its link with WNT/β-catenin signaling in CRC. We also investigated the role of BZW2 in CRC progression and showed that inhibition of cell growth and tumor progression after BZW2-knockdown was independent of *TP53, KRAS, BRAF, EGFR*, or microsatellite instability (MSI) status. We further reported the functional role of BZW2 in CRC experimental metastasis and its regulation by microRNA-98 and enhancer of zeste homolog 2 (EZH2) in addition to c-Myc. By use of gain- and loss-of-function experiments with CRC cell lines and mouse xenograft models, we identified prolyl 4-hydroxylase subunit alpha 1 (P4HA1), metastasis associated lung adenocarcinoma transcript 1 (MALAT1), and nuclear paraspeckle assembly transcript 1 (NEAT1) as downstream targets of BZW2. Additionally, for CRC cells expressing wild-type β-catenin, the WNT/β-catenin signaling pathway was regulated by BZW2. Since this study

suggests that BZW2 expression is regulated by EZH2, it is conceivable to target EZH2 with its FDA approved inhibitors to silence BZW2 expression. Furthermore, as BZW2 is a target for blocking CRC progression and metastasis, there is a rationale to develop small-molecule inhibitors of BZW2 that could serve as therapeutic agents for CRCs.

Materials and Methods

Analysis of human gene expression data

The differential expression of BZW2 between CRC and adjacent normal tissues was analyzed on August 2022 using the UALCAN portal (http://ualcan.path.uab.edu). Pearson's correlation coefficient values and a boxplot for finding gene correlation of BZW2 and EZH2 were built-in UALCAN (8). The Oncomine database (https://www.oncomine.org) was used in August 2022 for the comparison of BZW2 and EZH2 expression in CRCs relative to normal/benign colonic tissues.

Clinical tissue specimens

Formalin-fixed paraffin-embedded (FFPE) (n=169) and frozen archival cancer specimens (n=134) and their adjacent noncancerous/benign tissue specimens were collected from CRC patients by the Anatomic Pathology Division of the University of Alabama at Birmingham (UAB). The study includes a natural proportion of representation of patients (for age, race, and gender) who were admitted to the UAB hospital and excluded children under age 18. The study methodologies were performed in accordance with the standards set by the Declaration of Helsinki. The UAB Institutional Review Board (IRB#090513004) has approved for utilization of remnants of diagnostic CRC specimens, and an informed consent waiver was granted by the IRB. FFPE tumor specimens were processed for immunohistochemical (IHC) analyses, and frozen tissue specimens for RNA and protein analyses.

Cell lines and media

CRC cell lines (HCT116, SW480, HT29, and RKO) and CRL1807 SV40-transformed normal colon cells were obtained from ATCC (Manassas, VA). McCoy's medium (Corning™ Cellgro™, Fisher Scientific Co., Pittsburgh, PA) was used to grow these four CRC cell lines exhibiting various statuses of *TP53, KRAS, BRAF, EGFR, β-catenin*, and MSI (Supplementary Table S1). To grow CRL1807 SV40-transformed normal colon cells, fetal bovine serum (10%) (FBS, ThermoFisher Scientific, Carlsbad, CA) and penicillin-streptomycin were added to DMEM high-glucose medium and incubated at 5% CO_2 levels. Short tandem repeat DNA profiling was performed to authenticate cell lines and regularly tested for mycoplasma. The *BZW2* gene was packaged in pGreenPuro™ shRNA expression lentivectors (Systembio, Palo Alto, CA) by the UAB Neuroscience NINDS Protein Core (P30 NS47466). BZW2, P4HA1, and EZH2 shRNA sequences are provided in Supplementary Table S2.

Quantitative real-time PCR (qRT-PCR)

Total RNA was isolated by use of RNeasy mini kits (Zymo Research, Irvine, CA), and Superscript III Reverse Transcriptase (Invitrogen, Carlsbad, CA) was used for synthesis

of complementary DNA (cDNA) from CRC tissues and cell lines as described earlier (9). Integrated DNA Technologies (Coralville, IA) provided primers for SYBR green qRT-PCR to determine the mRNA expression of genes. For normalization, β-actin was used as a control. A list of primers is provided in Supplementary Table S3.

Immunohistochemical (IHC) analysis

BZW2 protein expression in CRC tissues was measured by IHC as described earlier (9, 10). In brief, tissue specimens were subjected to deparaffinization in xylene and rehydration by an alcohol series, followed by antigen retrieval by boiling slides with citric acid buffer solution. Subsequently, endogenous peroxidase was blocked by incubating the sections in BLOXALL solution (Vector Laboratories, Burlingame, CA). Normal horse serum was used to block the non-specific binding and sections were probed with polyclonal anti-BZW2 antibody (Supplementary Table S4). Further, slides were probed with ImmPRESS horseradish peroxidase anti-rabbit IgG (Vector laboratories, Burlingame, CA) as a secondary antibody. To assess immunoreactivity, diaminobenzidine (Vector laboratories, Burlingame, CA) was used, followed by counterstaining with Hematoxylin (Vector laboratories, Burlingame, CA).

Immunoblot analysis

As described earlier (11, 12), immunoblot analysis was performed using NuPAGE™ 4–12% Bis-Tris Midi Protein Gels, 20-well (ThermoFisher Scientific, Carlsbad, CA) for separation of proteins, followed by transfer onto Immobilon-P PVDF membranes (EMD Millipore, Billerica, MA). The membranes were incubated for 1 hour in blocking buffer (Tris-buffered saline, 0.1% Tween, TBS-T; 5% nonfat dry milk) followed by incubation with a primary antibody overnight at 4°C. Further, the preparations were probed with a horseradish peroxidase-conjugated secondary antibody, and Luminata™ Crescendo chemiluminescence Western blotting substrate (EMD Millipore, Billerica, MA) was used to detect signals; signal acquisition was assessed with an Amersham Imager 600RGB (GE Healthcare Life Sciences, Chicago, IL). A primary antibody list is provided in Supplementary Table S4.

RNA interference

For gene silencing experiments, pGreenPuro™ shRNA expression lentivectors (Systembio, Palo Alto, CA) consisting of BZW2 or P4HA1 shRNA or non-targeting (NT) controls were infected into CRC cells, and stable cell lines were generated by selection with medium containing 1 μg/ml puromycin (ThermoFisher Scientific, Carlsbad, CA) as described previously (13). The sequence details of shRNAs are provided in Supplemental Table S2. Knockdown efficiency was tested using immunoblot analyses. Stable puromycin-selected cells were used for cell-based assays.

Cell proliferation and colony formation studies

As described previously (14), CRC cells (2×10^3) with stable BZW2 shRNA or control NT shRNA were seeded into triplicate wells of 12-well plates to determine cell proliferation. At day 2, 4, and 6 post-transfection, cells were trypsinized and counted with a Z2 Coulter particle counter (Beckman Coulter, Brea, CA). To assess the colony formation capacity of

cells after BZW2-knockdown, 1×10^3 CRC cells with stable BZW2 or NT shRNA were seeded into 6-well plates in triplicate wells as described previously (12). After 10 days, cell colonies were fixed with 5% glutaraldehyde and stained with crystal violet (Sigma-Aldrich, St. Louis, MO). An Amersham Imager 600RGB (GE Healthcare Life Sciences, Pittsburgh, PA) was used to collect images of the colonies in 6-well plates.

Invasion assay

To evaluate cell invasion after BZW2-knockdown in CRC cells, we used Corning BioCoat™ Matrigel Transwell invasion chambers (Corning, New York, NY) as described (9). CRC cells (5×10^4) with stable BZW2-knockdown or control NT shRNA cells were seeded in the upper chambers with serum-free media; the lower chambers were filled with media containing FBS, an inducer of cell invasion. Invading cells that migrated to the lower side of the membranes were fixed with 5% glutaraldehyde and stained with crystal violet. Images were taken with a phase-contrast microscope.

3D spheroid model

Cell spheroid formation was evaluated as described previously (10, 12) using the Cultrex® 3D spheroid BME cell invasion assay (Trevigen, Gaithersburg, MD). Briefly, 5×10^3 cells were seeded into 96-well ultra-low attachment plates with 5 μl of Spheroid Formation ECM. Invasion matrix was added to the wells after 72 hours of incubation. FBS-supplemented media was added after 1 hour, and plates were incubated for 4 days. Images were taken with a 4x objective.

Tumor growth and an experimental metastasis model

To assess the role of BZW2 in tumor growth and metastasis, 6-week-old NOD/SCID/IL2γ-receptor null (NSG) mice (both male and female) were used to perform xenograft and metastasis studies as described previously (12, 14). Animal experiment protocols were approved by the UAB Institutional Animal Care and Use Committee (IACUC) (Approval Number: 21182), and all procedures were conducted in compliance with the IACUC. To determine tumor growth, HCT116 and SW480 cells with stable knockdown containing a non-targeting vector or BZW2 shRNA (1.0×10^6) or RKO cells stably overexpressing BZW2 (2.0×10^6) were injected subcutaneously into the right dorsal flanks of mice (n=6 for each group). Tumor growth was measured weekly by digital Vernier calipers, and tumor volume (mm^3) was calculated using the formula: (0.52) × (length) × ($width^2$). Mice were sacrificed at the end of the experiment, and tumors were excised, photographed, and weighed.

For metastasis experiments, as described previously (10), tail injections (were performed with mice bearing HT29 cells with BZW2 shRNA or NT shRNA (0.5×10^6) or RKO cells stably overexpressing BZW2 (0.5×10^6) and carrying a luciferase expression construct. At 10 minutes after luciferin injections, bioluminescence imaging was accomplished for mice using an IVIS Lumina III instrument (Perkin Elmer, Waltham, MA). At the end of the experiment, mouse lungs, liver, and hind-limb bones were dissected, and *ex vivo* analyses were performed.

Statistical analysis

Data were presented as means ± standard deviation for triplicates. Student's t-test (two-tailed) was used to perform comparisons of two groups. A *P*-value of <0.05 was considered statistically significant. Analysis of data was performed using χ^2 tests for categorical variables and t-tests for continuous variables. BZW2 IHC scores were categorized as low/high using the cutoff value of 0.41 (median IHC for normal samples). Comparison of paired tumor to normal IHC across clinical variables was evaluated with a Wilcoxon signed-rank test. All analyses were conducted in R 3.6.2., package.

Data availability

The RNA-seq data reported here are publicly available from the NCBI Gene Expression Omnibus (GEO) with accession number GSE227069. All the other data generated in this study are available upon request.

Results

BZW2 overexpression in CRCs is independent of tumor stage, tumor type, race/ethnicity, sex, and age

Examination of data in the publicly available UALCAN website (8) revealed BZW2 overexpression in CRCs (n=286) compared to normal colorectal tissues (n=41) (Supplementary Fig. S1A). Examination of these data according to the pathologic tumor stage showed overexpression of BZW2 in all CRC stages (Supplementary Fig. S1B). Our qRT-PCR analysis of BZW2 mRNA expression in the frozen CRC cohort (n=134) confirmed overexpression of BZW2 in CRCs (P<0.0001) relative to their corresponding normal/benign tissues (n=134) (Fig. 1A). UALCAN data for CRCs showed that overexpression of BZW2 was independent of patient's race (Supplementary Fig. S1C), sex (Supplementary Fig. S1D), and age (Supplementary Fig. S1E). Our in-house validation qRT-PCR data showed that BZW2 was overexpressed across pathologic stage (Fig. 1B) and patient's race (Caucasian vs African American) (Supplementary Fig. S1F), sex (male vs female) (Supplementary Fig. S1G), and age groups (21–40 years, 41–60 years, 61–80 years, and 81–100 years) (Supplementary Fig. S1H). Further, we explored the prognostic significance of BZW2 expression using UALCAL (TCGA) database. As illustrated by Kaplan–Meier survival curves, high expression of BZW2 was associated with poor survival of CRC patients (log rank, P = 0.017) (Fig. 1C). Thus, overexpression of BZW2 mRNA expression is associated with aggressive features of CRCs.

Protein expression profiles, assessed by Western blotting of BZW2 in matched tissue pairs of CRCs and adjacent benign tissues, revealed that BZW2 is overexpressed in all CRC tissues tested, irrespective of the pathologic stage of the tumor (Fig. 1D). Protein expression, determined by IHC, of BZW2 in matched pairs of CRC tissue and adjacent benign tissues (Supplementary Fig. S2A) revealed that BZW2 overexpression was present in most CRC tumor tissues irrespective of histologic type (Supplementary Fig. S2B), pathologic stage (Supplementary Fig. S2C), differentiation (Supplementary Fig. S2D), tumor location (Supplementary Fig. S2E), patient race (Supplementary Fig. S2F), sex, (Supplementary Fig. S2G), or *TP53* mutational status (Supplementary Fig. S2H). The CRC tissues used

in this study were previously evaluated for *TP53* mutational status (15). Additional testing of tumor BZW2 high/low expression categories found no significant differences by race, sex, stage, tumor location, differentiation, histologic type, or *TP53* mutational status (Supplementary Table S5). BZW2 staining was evident in the cytoplasm but not in the nuclei of adenomas and invasive adenocarcinomas relative to normal/benign colorectal tissues (Fig. 1E). Based on histology, BZW2 expression was present in mucinous and non-mucinous adenocarcinomas (Fig. 1F). These results demonstrate that BZW2 overexpression is involved in progression of all histologic/phenotypes of CRCs.

BZW2-knockdown reduces CRC cell growth, invasion, and tumor progression independent of TP53, KRAS, BRAF, EGFR, and MSI status

To assess the effects of BZW2-knockdown, a lentivirus-mediated stable shRNA knockdown strategy was used for loss-of-function studies. By immunoblot analyses, the knockdown efficiency of BZW2 by shRNA was validated (Fig. 2A). Then the functional role of BZW2 in CRC progression was assessed. Following BZW2 shRNA transfection, there was less colony formation by CRC cells relative to cells transfected with control non-targeting (NT) shRNA (NT shRNA) (Fig. 2B).

We used Transwell membrane assays to determine if BZW2-knockdown affected the invasive potential of the CRC cell lines HCT116, SW480, and HT29. Although NT shRNA cells showed robust invasion, knockdown of BZW2 in cells inhibited invasion (Supplementary Fig. S3). Culture of 3D spheroids, which mimic tumor growth (16), showed that BZW2-knockdown resulted in smaller spheroids (Fig. 2C). Moreover, the expression of a stem cell-related gene, *Oct4*, which plays an important role in spheroid formation and invasion, was lower when BZW2 was silenced (Supplementary Fig. S4A). These results establish that BZW2-knockdown reduces CRC malignant phenotypes and that the effects are independent of the *TP53*, *KRAS*, *BRAF*, EGFR, or MSI status of CRC cells.

Xenografts were established for HCT116 and SW480 cells. Cells transfected with NT shRNA or BZW2 shRNA were injected into NSG mice subcutaneously. At termination of the experiments, mice were euthanized, and tumors were harvested. Relative growth of xenografts of HCT116 (Fig. 2D) and SW480 (Fig. 2E) cells in NSG mice showed that, relative to controls, the average volumes and weights of tumors from mice injected with BZW2-knockdown cells were smaller. Moreover, *Oct4* gene expression was lower in xenografts, confirming the *in vitro* observation and indicating that cancer stemness was lower in BZW2-knockdown cells as compared to NT shRNA cells (Supplementary Fig. S4B). These findings suggest that BZW2-knockdown reduces malignant phenotypes and tumor growth independent of the *TP53*, *KRAS*, *BRAF*, EGFR, or MSI status.

BZW2-knockdown reduces CRC metastasis

NSG mice were intravenously injected with luciferase-tagged HT29 cells transfected with NT shRNA or BZW2 shRNA. For four weeks, animals were monitored by bioluminescence imaging to assess metastasis. Imaging of the mice showed lower luminescence for BZW2-knockdown relative to control NT shRNA mice (Fig. 3A). Imaging showed lower luminescence activity in lungs, liver, and hind limb-bones excised from mice that were

injected with BZW2- knockdown cells relative to NT shRNA cells (Fig. 3B). Further, bone marrow cells isolated from hind limbs were cultured in puromycin-containing media to select GFP-labeled CRC cells that had disseminated into bone marrow. After 3 days of culture, there were more CRC cells exhibiting GFP in the cultures taken from NT shRNA cells relative to those for mice injected with HT29-BZW2 shRNA cells (Fig. 3C). Additionally, using immunofluorescent assays, we showed a bone marrow interaction with invading cancer cells. As described previously, preparations were stained for alkaline phosphatase (ALP, a marker of bone marrow cells) and for cytokeratin 8+18 (a marker of proliferative lesions), which validates the presence of metastatic cancer cells in bone (10). Immunofluorescence analysis showed that cancer cells had invaded bones in mice injected with NT shRNA HT29 cells as compared to cells transfected with BZW2 shRNA (Fig. 3D). For mice with NT shRNA cells, there were bone metastases that interrupted the bone remodeling process and caused bone degradation and osteolytic lesions; BZW2-knockdown decreased osteolytic lesions and reduced the tumor burden in bone. These data suggest that BZW2-knockdown in CRC cells inhibits their capacity for establishing metastases in immunodeficient mice.

BZW2 overexpression promotes CRC cell growth, tumor progression, and metastasis

With lentiviral transduction, BZW2 was stably expressed in RKO cells, which expressed low levels of BZW2, as confirmed by immunoblot analysis (Fig. 4A). Relative to controls, ectopic expression of BZW2 in RKO cells led to elevated cell proliferation (Fig. 4B), colony formation (Fig. 4C), cell invasion (Fig. 4D), and spheroid formation (Fig. 4E). These cells also showed higher mRNA expression of *Oct4* (Supplementary Fig. S4C), indicating a role for BZW2 in cancer stemness. This ectopic expression of BZW2 produced tumors with higher volumes and weights compared with RKO cells transduced with the vector alone (Fig. 4F). Furthermore, tail-vein injections of RKO cells stably expressing BZW2 showed more extensive metastasis as compared to cells transduced with the lenti-control (Fig. 4G). Gross examination showed that metastases were more frequent in liver and kidney (Fig. 4H). Thus, ectopic expression of BZW2 in CRC cells exhibiting low levels of BZW2 promotes cell growth, tumor progression, and metastasis.

P4HA1, MALAT1, and NEAT1 are downstream targets of BZW2 in CRC

To investigate BZW2-mediated effects, we used RNA sequencing to conduct gene expression profiling of HCT116, SW480, and HT29 cells with stably inhibited BZW2. In all three CRC cells, we identified various genes that were modulated upon BZW2-knockdown, including those for P4HA1 and the long non-coding RNAs (lncRNAs), MALAT1 and NEAT1 (Fig. 5A). Further, using qRT-PCR analyses, we validated these findings with HCT116, SW480, and HT29 cells with BZW2-knockdown and showed that MALAT1 and NEAT1 were downregulated (Fig. 5B). Also, we demonstrated lower mRNA expression of P4HA1, as determined by RNA sequencing of BZW2-knockdown cells (Fig. 5C). In addition, we found lower levels of MALAT1 and NEAT1 in xenografts developed from cells with BZW2-knockdown (Fig. 5D). Furthermore, there were lower levels of P4HA1 protein in BZW2-knockdown CRC cells (HCT116 and SW480) (Fig. 5E), indicating that P4HA1 is a downstream target of BZW2. Similarly, RKO xenografts established with ectopic expression of BZW2 showed higher levels of P4HA1, MALAT1, and NEAT1 relative to

xenografts of cells transduced with a lenti-control (Fig. 5F). To validate P4HA1 as the downstream target of BZW2, we silenced its expression in HCT116 cells and found that BZW2 levels were not lower (Fig. 5G). Since AKAP9 and Ago2 are downstream targets of MALAT1 (17, 18), we assessed the levels of these two targets in HCT116 and HT29 cells and found lower levels in BZW2-knockdown cells (Supplementary Fig. S5A) as well as in xenografts of BZW2-knockdown cells (Supplementary Fig. S5B). In contrast, there were higher levels of AKAP9 and Ago2 in RKO xenografts established with ectopic expression of BZW2 (Supplementary Fig. S5C). These findings confirm that P4HA1, MALAT1, and NEAT1 are downstream targets of BZW2, and they mediate BZW2 action in CRC progression.

c-Myc and miR-98 regulate BZW2 expression in CRC

Since BZW2 is a downstream target of MYC in osteosarcomas and human lymphomas (19), we investigated the role of MYC in BZW2 regulation. By use of UALCAN data, we found a positive correlation between MYC and BZW2 in CRC (correlation coefficient, CC = 0.49) (Supplementary Fig. S6). Additionally, GEO dataset analyses showed that, for LOVO CRC cells, MYC bound to the promoter of BZW2 (Fig. 6A). We used adenovirus to overexpress MYC in CRL1807 SV-40 transformed colon cells. Overexpression of MYC increased the RNA expression of BZW2 (Fig. 6B). Also, treatment of CRC cells with a selective bromodomain inhibitor, JQ1, which reduces MYC levels, resulted in lower expression of BZW2 protein (Fig. 6C). These data show that MYC regulates BZW2 expression in CRC cells.

Web-based miR-targetscan (http://www.targetscan.org/vert_72/) and miRNA.org tools were used to demonstrate that miR-98 potentially targets BZW2. The predicted binding site for miR-98 at the 3'-UTR of BZW2 is shown in Supplementary Fig. S7A. To confirm the binding of miR-98 to this 3'-UTR, we performed dual luciferase miR-reporter assays by designing wild-type and mutant target sites (Supplementary Fig. S7A). Co-transfection of luciferase reporter vectors containing the BZW2 wild-type along with an miR-98 mimic into HCT116 cells showed lower luciferase activity; there was less effect when cells were co-transfected with BZW2 mutant and pre-miR-98 (Supplementary Fig. S7B). To determine if miR-98 reduces endogenous BZW2, we transfected HCT116 and SW480 cells with miR-98. Overexpression of miR-98 in CRC cells reduced protein levels of BZW2 (Fig. 6D). To assess the biological function of miR-98, we evaluated the effects of miR-98 ectopic overexpression on malignant phenotypes of CRC cells. Overexpression of miR-98 in CRC cells inhibited cell proliferation (Fig. 6E), colony formation (Fig. 6F), and invasion (Fig. 6G). These results show that, in CRCs, miR-98 targets BZW2 and that its suppressive functions are associated with inhibition of malignant phenotypes of CRC.

EZH2 regulates BZW2 expression in CRC

Since there is downregulation of miR-98 in CRCs (20), and EZH2 regulates miR-98 (21), we investigated the mechanism of downregulation of miR-98 through EZH2 in CRC by evaluating miR-98 expression in CRC cells with EZH2-knockdown. There was higher expression of miR-98 in cells with EZH2-knockdown (Fig. 7A). When cells were treated with an inhibitor targeting EZH2, GSK126, there were higher levels of miR-98 and lower

levels of BZW2, consistent with the regulation of BZW2 by EZH2 via miR-98 (Fig. 7B). Further, in evaluation of human CRCs, expression of miR-98 inversely correlated with EZH2 and BZW2 mRNA expression (Fig. 7C), indicating a role of EZH2 in regulation of BZW2. Thus, suggesting that, with use of an FDA-approved inhibitor of EZH2 (NCT01897571, tazemetostate) BZW2 can be indirectly targeted.

Evaluation of the Skrzypczak dataset (22) available in Oncomine showed a possible positive correlation between gene expression profiles of BZW2 and EZH2 (Supplementary Fig. S8A). TCGA (UALCAN) data analysis also showed a positive correlation between BZW2 and EZH2 (correlation coefficient, CC = 0.33) (Supplementary Fig. S8B). Since our prior study demonstrated that EZH2 regulates P4HA1 in CRC (13), and the present work showed that P4HA1 is a down-stream target of BZW2, we evaluated the association of BZW2 protein expression with EZH2 and P4HA1 in human CRCs and matched normal colon tissue lysates. Overexpression of EZH2, BZW2, and P4HA1 were evident in CRCs as compared to their corresponding normal/benign colon tissues, indicating a positive correlation among these molecules (Fig. 7D).

Inhibition of the WNT/β-catenin signaling pathway by BZW2-knockdown is dependent on the β-catenin status

As the WNT/β-catenin signaling pathway is involved in CRC progression (23), we determined if BZW2 regulates this pathway. HCT116 cells harbor a mutation in β-catenin but SW480 and RKO cells show a wild-type β-catenin status. For HCT116 xenografts established with cells with BZW2-knockdown, there were no changes in activation of β-catenin, cyclin D1, or TCF1 (Fig. 7E); SW480 xenografts showed lower activation of β-catenin, cyclin D1, and TCF1 in tumors with BZW2-knockdown (Figs. 7F). Moreover, RKO xenografts had low levels of BZW2, and, upon overexpression of BZW2, the RKO xenografts showed higher levels of active β-catenin, cyclin D1, and TCF1, indicating activation of the WNT/β-catenin signaling pathway (Fig. 7G). Further, we evaluated the levels of BZW2 and molecules of the WNT/β-catenin signaling pathway in human CRCs and showed higher expression of WNT/β-catenin-related molecules (Fig. 7H) and higher levels of BZW2. These results suggest that the WNT/β-catenin signaling pathway is regulated by BZW2 in CRCs that harbor wild-type β-catenin.

Discussion

In the present study, we showed that, consistent with a previous report (7), BZW2 levels were upregulated in CRC tissues, and that its knockdown lowered CRC progression (6, 7). Further, the novel findings of this study are a) overexpression of BZW2 in CRC was irrespective of pathologic stage, tumor location, differentiation, histologic type, *TP53* status, race, or sex; b) CRC cells with various molecular alterations (*TP53*, *KRAS*, *BRAF*, *EGFR*, or MSI) showed high levels of BZW2, and its knockdown led to lower cell proliferation, invasion, and growth, including xenograft tumor growth for cell lines with various molecular backgrounds. Thus, growth inhibition was not dependent on the molecular status of the cells; c) BZW2 overexpression was noted in human primary CRCs, and its knockdown in an experimental metastatic model delayed the onset of liver, lung, and bone metastases; d)

expression of BZW2 was regulated by miRNA-98, c-Myc, and EZH2; e) BZW2 regulated P4HA1 and the long non-coding RNAs, MALAT1 and NEAT1; and f) BZW2 was involved in activation of the WNT/β-catenin signaling pathway in CRC cells harboring wild-type β-catenin. Since metastasis is a predominant cause of CRC deaths (24), our findings related to reducing metastasis by inhibiting BZW2 suggest that BZW2 might be a therapeutic target for CRC metastasis.

Examination of publicly available datasets and our in-house validation of human CRC tissues revealed overexpression of BZW2, at RNA and protein levels, in CRCs compared to their adjacent normal/benign colon tissues as shown previously (7). Additionally, our findings suggested that the overexpression of BZW2 was regardless of CRC pathologic stage, primary tumor location, histologic type, grading, or patient's race, sex, or age. Furthermore, high expression of BZW2 was associated with poor survival of CRC patients. Thus, BZW2 overexpression is - related to aggressive features of CRCs.

As demonstrated earlier (6, 7), our studies that assessed the functional role of BZW2 have established that BZW2-knockdown reduces CRC malignant phenotypes (cell proliferation, colony formation, invasion/motility, and cell growth). Further, our investigations have shown that silencing of BZW2 reduces malignant phenotypes, tumor growth, and metastasis, effects that are independent of the *TP53, KRAS, BRAF, EGFR*, or MSI status of CRC cells. Also, in BZW2-knockdown studies, bioluminescence imaging showed less metastasis, particularly in lungs, liver, and bones, which are predominant sites of CRC metastasis leading to deaths (24). Our studies also showed that BZW2-knockdown decreased osteolytic lesions and reduced tumor burden in bone, suggesting that BZW2 inhibition reduces CRC metastases.

Using a cell line (RKO) with low BZW2 expression, we confirmed the effects of BZW2 on CRC progression through gain- and loss-of-function experiments. Overexpression of BZW2 increased cell proliferation and tumor growth. BZW2-knockdown lowered the cancer stemness marker, *OCT4*, and upregulation of BZW2 in RKO xenografts increased the expression of *OCT4*, indicating a role of BZW2 in cancer stemness. These data indicate that BZW2 functions as an oncogene during CRC progression.

RNA sequencing analysis revealed that MALAT1, NEAT1, and P4HA1 are downstream targets of BZW2. These targets were validated with cell cultures and xenografts developed from cells with BZW2-knockdown or with transduction of BZW2. Furthermore, expression of AKAP9, a downstream target of MALAT1 (18), was low in BZW2-knockdown CRC cells and xenografts; BZW2-overexpressing xenografts showed high expression of AKAP9. Of note, MALAT1 is overexpressed in various cancers, including those of the lung (25), bladder (26), breast (27), cervix (28), colorectum (29), esophagus (30), stomach (31), and prostate (32). NEAT1 is involved in the progression of CRC (33), pancreatic cancer (34), endometrial cancer (35), and breast cancer (36). P4HA1 is involved in the progression of breast cancer (37), hepatocellular carcinoma (38), pancreatic cancer (39), high-grade gliomas (40), prostate cancer (41), and oral squamous cell carcinomas (42). Our previous studies with CRC revealed that overexpression of P4HA1 is involved in metastasis and growth of PDX tumors (13). These findings suggest that BZW2 is involved in CRC progression through MALAT1, NEAT1, P4HA1, and other downstream targets.

A prior study has found that BZW2 is regulated by MYC to maintain tumorigenesis (19). In contrast, another study has reported that, for CRCs, c-Myc is a potential downstream effector of BZW2 (7). However, our results demonstrated that ectopic expression of MYC in SV-40-transformed CRL1807 normal colon cells lead to higher expression of BZW2. Moreover, a BRD4 inhibitor, JQ1, which suppresses MYC, produced lower levels of BZW2 in CRC cells exposed to JQ1. Furthermore, our GEO data analyses showed that, for CRC, MYC bound to the promoter of BZW2. These results establish that MYC regulates BZW2 expression.

With publicly available data, we found that miR-98, a member of the let-7 family, is a potential upstream regulator of BZW2. We showed that elevated expression of miR-98–5p targets BZW2 and reduces the malignant behavior of CRC cells. Cell proliferation, colony formation, and invasion were low in cells with ectopically overexpressed miR-98–5p. These results suggest that, in CRCs, miR-98 targets BZW2. miR-98 targets IL-6 and suppresses metastasis in melanoma (43), SALL4 in hepatocellular carcinoma (44), IGF1R in oral squamous cell carcinoma (45), Gab2 in breast cancer (46), and ITGB3 in non-small-cell lung cancer (47). Also, miR-98 inhibits CRC cell proliferation, invasion, and migration by downregulating CLDN1 (48). In addition, upregulation of miR-98 inhibits proliferation, migration, and invasion of pancreatic cancer cells by targeting the MAP4K4-mediated MAPK/ERK pathway (49). These reports and our findings demonstrate that, by targeting BZW2, miR-98 has a tumor suppressive role in CRCs.

Since miR-98 is repressed by EZH2 (21), we investigated the mechanism of downregulation of miR-98 through the epigenetic modifier and histone H3-K27-trimethylating enzyme, EZH2, by evaluating its expression in CRC cells with EZH2-knockdown. Consistent with the prior study, our results revealed that EZH2-knockdown increased miR-98 expression. Additionally, for CRC cells, EZH2-knockdown reduced the levels of BZW2, indicating that BZW2 was regulated by EZH2 via miR-98. Furthermore, with human CRC specimens, we found that expression of miR-98 inversely correlated with expression of EZH2 and BZW2. Thus, our investigations demonstrate a link between miR-98, EZH2, and BZW2, indicating that EZH2 regulates BZW2 expression through repressing miR-98.

Abnormal activation or dysregulation of the Wnt/β-catenin signaling pathway is present in 90% of CRCs (50). The activation of Wnt/β-catenin signaling could increase the amount of β-catenin protein in the nucleus, where it forms complexes with TCF/LEF to regulate expression of target genes (51). In addition, β-catenin mutation results in loss or downregulation of the β-catenin pathway and is involved in uncontrolled cell growth, neoplastic changes, and tumor development (52, 53). Knockdown of BZW2 led to the downregulation of β-catenin, TCF1, and cyclin D1 in CRC cells expressing wild-type β-catenin but not the mutant form of β-catenin. Further, overexpression of BZW2 activated the Wnt/β-catenin signaling pathway in CRC cells expressing wild-type β-catenin. Additionally, CRC specimens demonstrated a positive correlation between BZW2 and active-β-catenin. These findings revealed that activation of the Wnt/β-catenin signaling pathway by BZW2 is dependent on β-catenin status.

Conclusions

In sum, the present study revealed that BZW2 expression was upregulated in human CRC tissues. In CRC cells, BZW2 acted as an oncogene regardless of the cellular status of *TP53, KRAS*, *BRAF*, EGFR, or MSI, and it promoted experimental metastases of CRC to liver, lung, and bone. Findings of the present study showed that BZW2 was regulated by miR-98, c-MYC, and EZH2. We identified collagen modifying enzyme P4HA1 and the long non-coding RNAs, MALAT1 and NEAT1, as its downstream targets and showed that overexpression of BZW2 dysregulates WNT/β-catenin signaling, which is dependent on wild-type β-catenin. The results provide evidence of BZW2 regulation, its oncogenic functions, and as a molecular target for blocking CRC progression. Additionally, findings support the rational to develop small molecule inhibitors of BZW2, which could serve as therapeutic agents for CRC. Further, FDA-approved EZH2 small molecule inhibitors (e.g. tazemetostate), can indirectly target BZW2 and serve as a therapeutic option to block BZW2 mediated effects in CRC.

Supplementary Material

Refer to Web version on PubMed Central for supplementary material.

Acknowledgments

We thank Dr. Donald Hill, a member of the UAB O'Neal Comprehensive Cancer Center (CCC), for his editorial assistance. We acknowledge the technical support of Ms. Briana Huffman, a student from Stillman College who participated in the summer research program of UAB, for performing IHC on a set of samples. These studies were supported by a grant 5U54CA118948 of Centre to Reduce Cancer Health Disparities of the National Cancer Institute (UM), its full project (SV) and by institutional impact funds (Department of Pathology and School of Medicine of the University of Alabama at Birmingham) awarded to UM. We acknowledge the grants funded for the Tissue Biorepository, high resolution imaging facility and animal imaging facility of the UAB O'Neal CCC (P30CA013148 and 1S10OD021697) and for the UAB Neuroscience NINDS Protein Core (P30 NS47466).

References

1. Siegel RL, Miller KD, Goding Sauer A, Fedewa SA, Butterly LF, Anderson JC, et al. Colorectal cancer statistics, 2021. CA Cancer J Clin. 2021.
2. Singh CR, Watanabe R, Zhou D, Jennings MD, Fukao A, Lee B, et al. Mechanisms of translational regulation by a human eIF5-mimic protein. Nucleic Acids Res. 2011;39(19):8314–28. [PubMed: 21745818]
3. Cheng DD, Li SJ, Zhu B, Yuan T, Yang QC, Fan CY. Downregulation of BZW2 inhibits osteosarcoma cell growth by inactivating the Akt/mTOR signaling pathway. Oncol Rep. 2017;38(4):2116–22. [PubMed: 28791373]
4. Jin X, Liao M, Zhang L, Yang M, Zhao J. Role of the novel gene BZW2 in the development of hepatocellular carcinoma. J Cell Physiol. 2019.
5. Gao H, Yu G, Zhang X, Yu S, Sun Y, Li Y. BZW2 gene knockdown induces cell growth inhibition, G1 arrest and apoptosis in muscle-invasive bladder cancers: A microarray pathway analysis. J Cell Mol Med. 2019;23(6):3905–15. [PubMed: 30932331]
6. Huang L, Chen S, Fan H, Ai F, Sheng W. BZW2 promotes the malignant progression of colorectal cancer via activating the ERK/MAPK pathway. J Cell Physiol. 2020;235(5):4834–42. [PubMed: 31643092]
7. Sato K, Masuda T, Hu Q, Tobo T, Gillaspie S, Niida A, et al. Novel oncogene 5MP1 reprograms c-Myc translation initiation to drive malignant phenotypes in colorectal cancer. EBioMedicine. 2019;44:387–402. [PubMed: 31175057]

8. Chandrashekar DS, Bashel B, Balasubramanya SAH, Creighton CJ, Ponce-Rodriguez I, Chakravarthi B, et al. UALCAN: A Portal for Facilitating Tumor Subgroup Gene Expression and Survival Analyses. Neoplasia. 2017;19(8):649–58. [PubMed: 28732212]
9. Agarwal S, Chakravarthi B, Behring M, Kim HG, Chandrashekar DS, Gupta N, et al. PAICS, a Purine Nucleotide Metabolic Enzyme, is Involved in Tumor Growth and the Metastasis of Colorectal Cancer. Cancers (Basel). 2020;12(4).
10. Agarwal S, Behring M, Kim HG, Chandrashekar DS, Chakravarthi B, Gupta N, et al. TRIP13 promotes metastasis of colorectal cancer regardless of p53 and microsatellite instability status. Mol Oncol. 2020;14(12):3007–29. [PubMed: 33037736]
11. Agarwal S, Behring M, Hale K, Al Diffalha S, Wang K, Manne U, et al. MTHFD1L, A Folate Cycle Enzyme, Is Involved in Progression of Colorectal Cancer. Transl Oncol. 2019;12(11):1461–7. [PubMed: 31421459]
12. Agarwal S, Afaq F, Bajpai P, Kim HG, Elkholy A, Behring M, et al. DCZ0415, a small-molecule inhibitor targeting TRIP13, inhibits EMT and metastasis via inactivation of the FGFR4/STAT3 axis and the Wnt/β-catenin pathway in colorectal cancer. Mol Oncol. 2022;16(8):1728–45. [PubMed: 35194944]
13. Agarwal S, Behring M, Kim HG, Bajpai P, Chakravarthi B, Gupta N, et al. Targeting P4HA1 with a Small Molecule Inhibitor in a Colorectal Cancer PDX Model. Transl Oncol. 2020;13(4):100754. [PubMed: 32199274]
14. Agarwal S, Chakravarthi B, Kim HG, Gupta N, Hale K, Balasubramanya SAH, et al. PAICS, a De Novo Purine Biosynthetic Enzyme, Is Overexpressed in Pancreatic Cancer and Is Involved in Its Progression. Transl Oncol. 2020;13(7):100776. [PubMed: 32422575]
15. Katkoori VR, Jia X, Shanmugam C, Wan W, Meleth S, Bumpers H, et al. Prognostic significance of p53 codon 72 polymorphism differs with race in colorectal adenocarcinoma. Clin Cancer Res. 2009;15(7):2406–16. [PubMed: 19339276]
16. Zhang Q, Yu S, Lam MMT, Poon TCW, Sun L, Jiao Y, et al. Angiotensin II promotes ovarian cancer spheroid formation and metastasis by upregulation of lipid desaturation and suppression of endoplasmic reticulum stress. J Exp Clin Cancer Res. 2019;38(1):116. [PubMed: 30845964]
17. Yang MH, Hu ZY, Xu C, Xie LY, Wang XY, Chen SY, et al. MALAT1 promotes colorectal cancer cell proliferation/migration/invasion via PRKA kinase anchor protein 9. Biochim Biophys Acta. 2015;1852(1):166–74. [PubMed: 25446987]
18. Zhao M, Wang S, Li Q, Ji Q, Guo P, Liu X. MALAT1: A long non-coding RNA highly associated with human cancers. Oncol Lett. 2018;16(1):19–26. [PubMed: 29928382]
19. Wu CH, Sahoo D, Arvanitis C, Bradon N, Dill DL, Felsher DW. Combined analysis of murine and human microarrays and ChIP analysis reveals genes associated with the ability of MYC to maintain tumorigenesis. PLoS Genet. 2008;4(6):e1000090. [PubMed: 18535662]
20. Liu S, Zhou Y, Zhou Y, Wang J, Ji R. Mechanism of miR-98 inhibiting tumor proliferation and invasion by targeting IGF1R in diabetic patients combined with colon cancer. Oncol Lett. 2020;20(2):1719–26. [PubMed: 32724414]
21. Cao Q, Mani RS, Ateeq B, Dhanasekaran SM, Asangani IA, Prensner JR, et al. Coordinated regulation of polycomb group complexes through microRNAs in cancer. Cancer Cell. 2011;20(2):187–99. [PubMed: 21840484]
22. Skrzypczak M, Goryca K, Rubel T, Paziewska A, Mikula M, Jarosz D, et al. Modeling oncogenic signaling in colon tumors by multidirectional analyses of microarray data directed for maximization of analytical reliability. PLoS One. 2010;5(10).
23. Huang D, Du X. Crosstalk between tumor cells and microenvironment via Wnt pathway in colorectal cancer dissemination. World J Gastroenterol. 2008;14(12):1823–7. [PubMed: 18350618]
24. Guo X, Zhang C, Ma W, Tian F, Xu G, Han X, et al. Patterns of bone metastases in newly diagnosed colorectal cancer: a real-world analysis in the SEER database. Int J Colorectal Dis. 2019;34(3):533–43. [PubMed: 30617414]
25. Ji P, Diederichs S, Wang W, Boing S, Metzger R, Schneider PM, et al. MALAT-1, a novel noncoding RNA, and thymosin beta4 predict metastasis and survival in early-stage non-small cell lung cancer. Oncogene. 2003;22(39):8031–41. [PubMed: 12970751]

26. Fan Y, Shen B, Tan M, Mu X, Qin Y, Zhang F, et al. TGF-beta-induced upregulation of malat1 promotes bladder cancer metastasis by associating with suz12. Clin Cancer Res. 2014;20(6):1531–41. [PubMed: 24449823]
27. Zhao Z, Chen C, Liu Y, Wu C. 17beta-Estradiol treatment inhibits breast cell proliferation, migration and invasion by decreasing MALAT-1 RNA level. Biochem Biophys Res Commun. 2014;445(2):388–93. [PubMed: 24525122]
28. Guo F, Li Y, Liu Y, Wang J, Li Y, Li G. Inhibition of metastasis-associated lung adenocarcinoma transcript 1 in CaSki human cervical cancer cells suppresses cell proliferation and invasion. Acta Biochim Biophys Sin (Shanghai). 2010;42(3):224–9. [PubMed: 20213048]
29. Ji Q, Zhang L, Liu X, Zhou L, Wang W, Han Z, et al. Long non-coding RNA MALAT1 promotes tumour growth and metastasis in colorectal cancer through binding to SFPQ and releasing oncogene PTBP2 from SFPQ/PTBP2 complex. Br J Cancer. 2014;111(4):736–48. [PubMed: 25025966]
30. Hu L, Wu Y, Tan D, Meng H, Wang K, Bai Y, et al. Up-regulation of long noncoding RNA MALAT1 contributes to proliferation and metastasis in esophageal squamous cell carcinoma. J Exp Clin Cancer Res. 2015;34:7. [PubMed: 25613496]
31. Okugawa Y, Toiyama Y, Hur K, Toden S, Saigusa S, Tanaka K, et al. Metastasis-associated long non-coding RNA drives gastric cancer development and promotes peritoneal metastasis. Carcinogenesis. 2014;35(12):2731–9. [PubMed: 25280565]
32. Ren S, Liu Y, Xu W, Sun Y, Lu J, Wang F, et al. Long noncoding RNA MALAT-1 is a new potential therapeutic target for castration resistant prostate cancer. J Urol. 2013;190(6):2278–87. [PubMed: 23845456]
33. Luo Y, Chen JJ, Lv Q, Qin J, Huang YZ, Yu MH, et al. Long non-coding RNA NEAT1 promotes colorectal cancer progression by competitively binding miR-34a with SIRT1 and enhancing the Wnt/beta-catenin signaling pathway. Cancer Lett. 2019;440–441:11–22.
34. Cao J, Zhang Y, Yang J, He S, Li M, Yan S, et al. NEAT1 regulates pancreatic cancer cell growth, invasion and migration though mircroRNA-335–5p/c-met axis. Am J Cancer Res. 2016;6(10):2361–74. [PubMed: 27822425]
35. Dong P, Xiong Y, Yue J, Xu D, Ihira K, Konno Y, et al. Long noncoding RNA NEAT1 drives aggressive endometrial cancer progression via miR-361-regulated networks involving STAT3 and tumor microenvironment-related genes. J Exp Clin Cancer Res. 2019;38(1):295. [PubMed: 31287002]
36. Shin VY, Chen J, Cheuk IW, Siu MT, Ho CW, Wang X, et al. Long non-coding RNA NEAT1 confers oncogenic role in triple-negative breast cancer through modulating chemoresistance and cancer stemness. Cell Death Dis. 2019;10(4):270. [PubMed: 30894512]
37. Xiong G, Stewart RL, Chen J, Gao T, Scott TL, Samayoa LM, et al. Collagen prolyl 4-hydroxylase 1 is essential for HIF-1alpha stabilization and TNBC chemoresistance. Nature communications. 2018;9(1):4456.
38. Feng G, Shi H, Li J, Yang Z, Fang R, Ye L, et al. MiR-30e suppresses proliferation of hepatoma cells via targeting prolyl 4-hydroxylase subunit alpha-1 (P4HA1) mRNA. Biochem Biophys Res Commun. 2016;472(3):516–22. [PubMed: 26966067]
39. Cao XP, Cao Y, Li WJ, Zhang HH, Zhu ZM. P4HA1/HIF1alpha feedback loop drives the glycolytic and malignant phenotypes of pancreatic cancer. Biochem Biophys Res Commun. 2019;516(3):606–12. [PubMed: 31239153]
40. Hu WM, Zhang J, Sun SX, Xi SY, Chen ZJ, Jiang XB, et al. Identification of P4HA1 as a prognostic biomarker for high-grade gliomas. Pathol Res Pract. 2017;213(11):1365–9. [PubMed: 28964577]
41. Chakravarthi BV, Pathi SS, Goswami MT, Cieslik M, Zheng H, Nallasivam S, et al. The miR-124-prolyl hydroxylase P4HA1-MMP1 axis plays a critical role in prostate cancer progression. Oncotarget. 2014;5(16):6654–69. [PubMed: 25115393]
42. Kappler M, Kotrba J, Kaune T, Bache M, Rot S, Bethmann D, et al. P4HA1: A single-gene surrogate of hypoxia signatures in oral squamous cell carcinoma patients. Clin Transl Radiat Oncol. 2017;5:6–11. [PubMed: 29594211]

43. Li F, Li XJ, Qiao L, Shi F, Liu W, Li Y, et al. miR-98 suppresses melanoma metastasis through a negative feedback loop with its target gene IL-6. Exp Mol Med. 2014;46:e116. [PubMed: 25277211]
44. Zhou W, Zou B, Liu L, Cui K, Gao J, Yuan S, et al. MicroRNA-98 acts as a tumor suppressor in hepatocellular carcinoma via targeting SALL4. Oncotarget. 2016;7(45):74059–73. [PubMed: 27677076]
45. Du Y, Li Y, Lv H, Zhou S, Sun Z, Wang M. miR-98 suppresses tumor cell growth and metastasis by targeting IGF1R in oral squamous cell carcinoma. Int J Clin Exp Pathol. 2015;8(10):12252–9. [PubMed: 26722410]
46. Shi XY, Wang H, Wang W, Gu YH. MiR-98–5p regulates proliferation and metastasis of MCF-7 breast cancer cells by targeting Gab2. Eur Rev Med Pharmacol Sci. 2020;24(21):10914. [PubMed: 33215398]
47. Ni R, Huang Y, Wang J. miR-98 targets ITGB3 to inhibit proliferation, migration, and invasion of non-small-cell lung cancer. Onco Targets Ther. 2015;8:2689–97. [PubMed: 26445551]
48. Zheng YF, Luo J, Gan GL, Li W. Overexpression of microRNA-98 inhibits cell proliferation and promotes cell apoptosis via claudin-1 in human colorectal carcinoma. J Cell Biochem. 2019;120(4):6090–105. [PubMed: 30506722]
49. Fu Y, Liu X, Chen Q, Liu T, Lu C, Yu J, et al. Downregulated miR-98–5p promotes PDAC proliferation and metastasis by reversely regulating MAP4K4. J Exp Clin Cancer Res. 2018;37(1):130. [PubMed: 29970191]
50. Liu Y, Yu J, Xie Y, Li M, Wang F, Zhang J, et al. EZH2 regulates sFRP4 expression without affecting the methylation of sFRP4 promoter DNA in colorectal cancer cell lines. Exp Ther Med. 2020;20(5):33. [PubMed: 32952624]
51. Tang Q, Chen J, Di Z, Yuan W, Zhou Z, Liu Z, et al. TM4SF1 promotes EMT and cancer stemness via the Wnt/beta-catenin/SOX2 pathway in colorectal cancer. J Exp Clin Cancer Res. 2020;39(1):232. [PubMed: 33153498]
52. Ilyas M, Tomlinson IP, Rowan A, Pignatelli M, Bodmer WF. Beta-catenin mutations in cell lines established from human colorectal cancers. Proc Natl Acad Sci U S A. 1997;94(19):10330–4. [PubMed: 9294210]
53. El-Bahrawy M, Poulsom R, Rowan AJ, Tomlinson IT, Alison MR. Characterization of the E-cadherin/catenin complex in colorectal carcinoma cell lines. Int J Exp Pathol. 2004;85(2):65–74. [PubMed: 15154912]

Implications:

FDA-approved small molecule inhibitors of EZH2 can indirectly target BZW2 and since BZW2 functions as an oncogene, these inhibitors could serve as therapeutic agents for CRC.

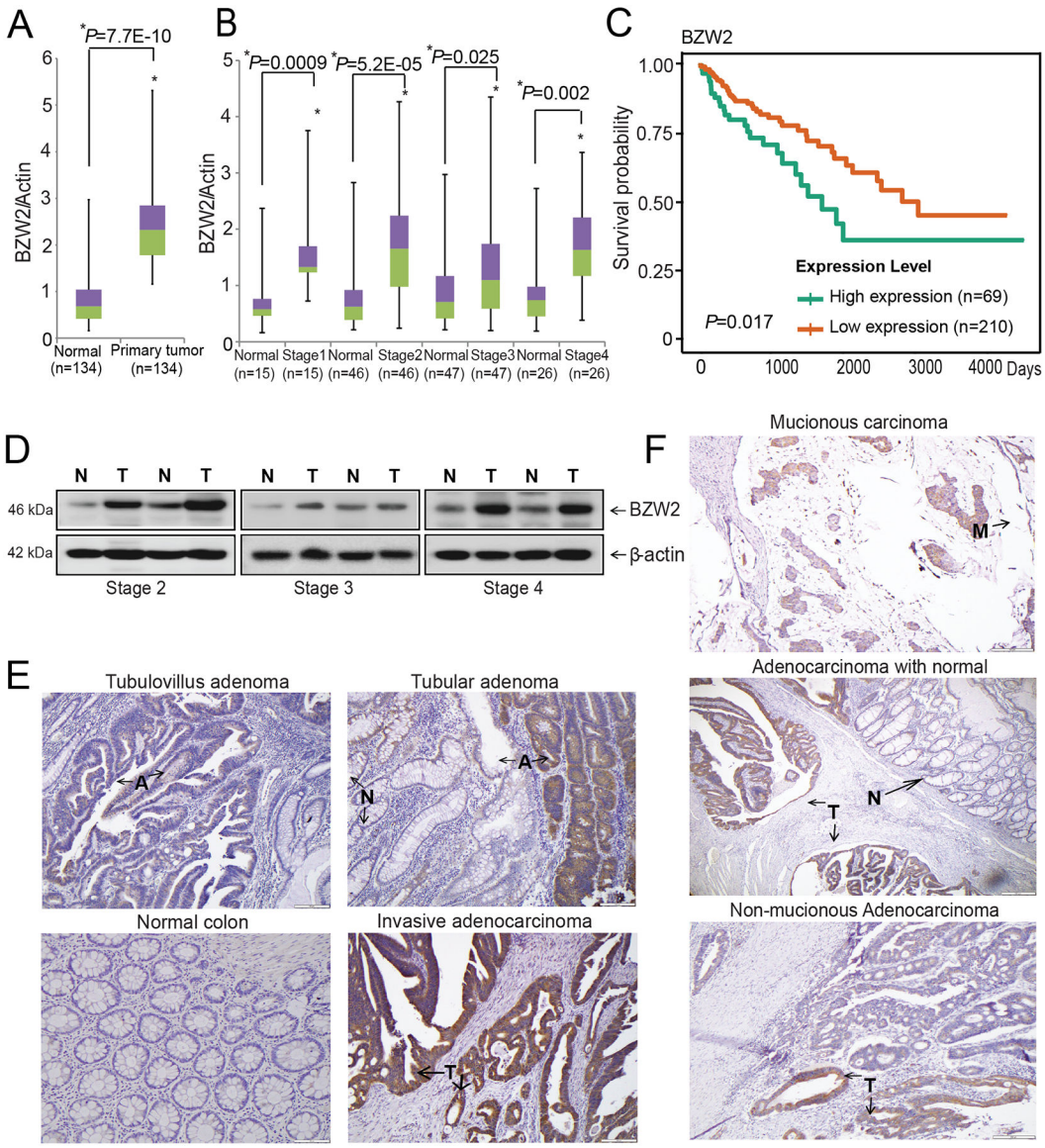

Figure 1.

BZW2 upregulation in CRC. **A**, BZW2 RNA expression in frozen CRC tissues of whole cohort with matched normals was quantified by qRT-PCR using specific primers. Histograph presenting group comparisons of relative BZW2 RNA expression in frozen paired normal (n=134) and tumor tissues (n=134) of CRC patients. **B**, In-house validation qRT-PCR analysis showing BZW2 expression in various pathologic stages (Stage 1, n=15; Stage 2, n=46; Stage 3, n=47; and Stage 4, n=26). **C**, Kaplan-Meier curves for CRC-specific survival with low and high BZW2 expression according to data from TCGA (log rank, P=0.017). **D**, Western blot analyses showing BZW2 levels in frozen CRCs and in paired adjacent non-cancerous tissues with respect to the stage of cancer. **E & F**, IHC staining showing the BZW2 expression in adjacent non-tumor tissue (denoted by N), tubule-villus adenoma, tubular adenoma (denoted by A), mucinous carcinoma (denoted by M), adenocarcinoma, and invasive CRC tissues. Hematoxylin was used for nuclear staining. Scale bar, 100 μm.

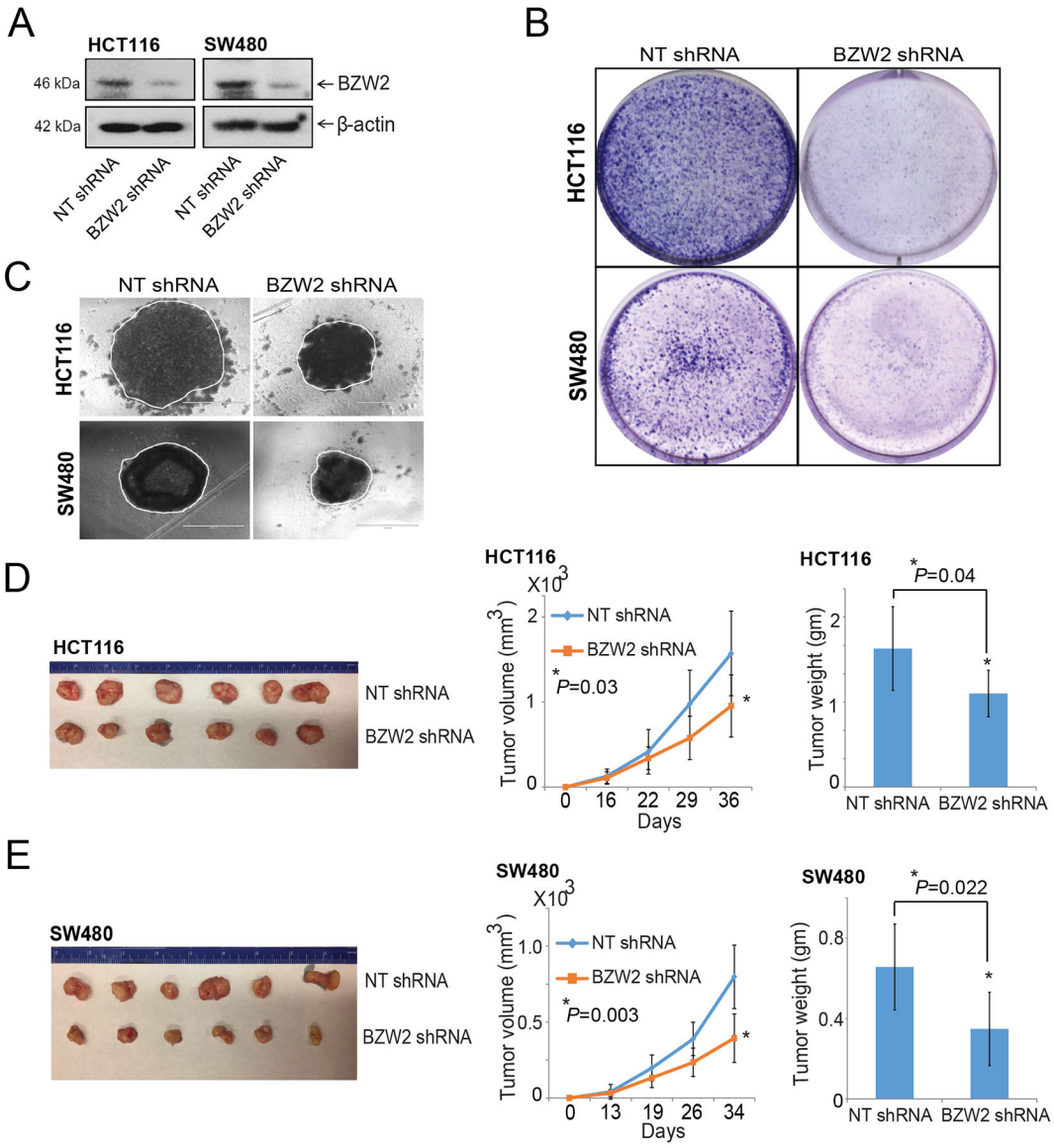

Figure 2.

BZW2 involvement in the proliferation, spheroid formation, and tumor growth of CRC cells. **A**, The expression of BZW2 was measured by Western blots after BZW2-knockdown in CRC cells, HCT116 and SW480. β-Actin was used as a loading control. **B**, Representative photographs of the colony formation assay for NT shRNA and BZW2-knockdown CRC cells. **C**, Phase-contrast microscopy images of CRC spheroids of NT shRNA and BZW2-knockdown cells (scale bar, 1000 μm). NSG mice were injected subcutaneously with HCT116 or SW480 cells (1.0×10^6/mouse) manifesting various TP53 status with NT shRNA or BZW2 shRNA. **D**, Representative images of tumors at the end of the experiment showing HCT116, and **E**, SW480 xenograft tumors exhibiting control NT shRNA and BZW2 shRNA. Gross observation of BZW2 shRNA xenografts showing smaller tumors for CRC cells as compared to those of NT shRNA xenografts. Tumor volumes and tumor weights were measured and plotted as means ± SD.

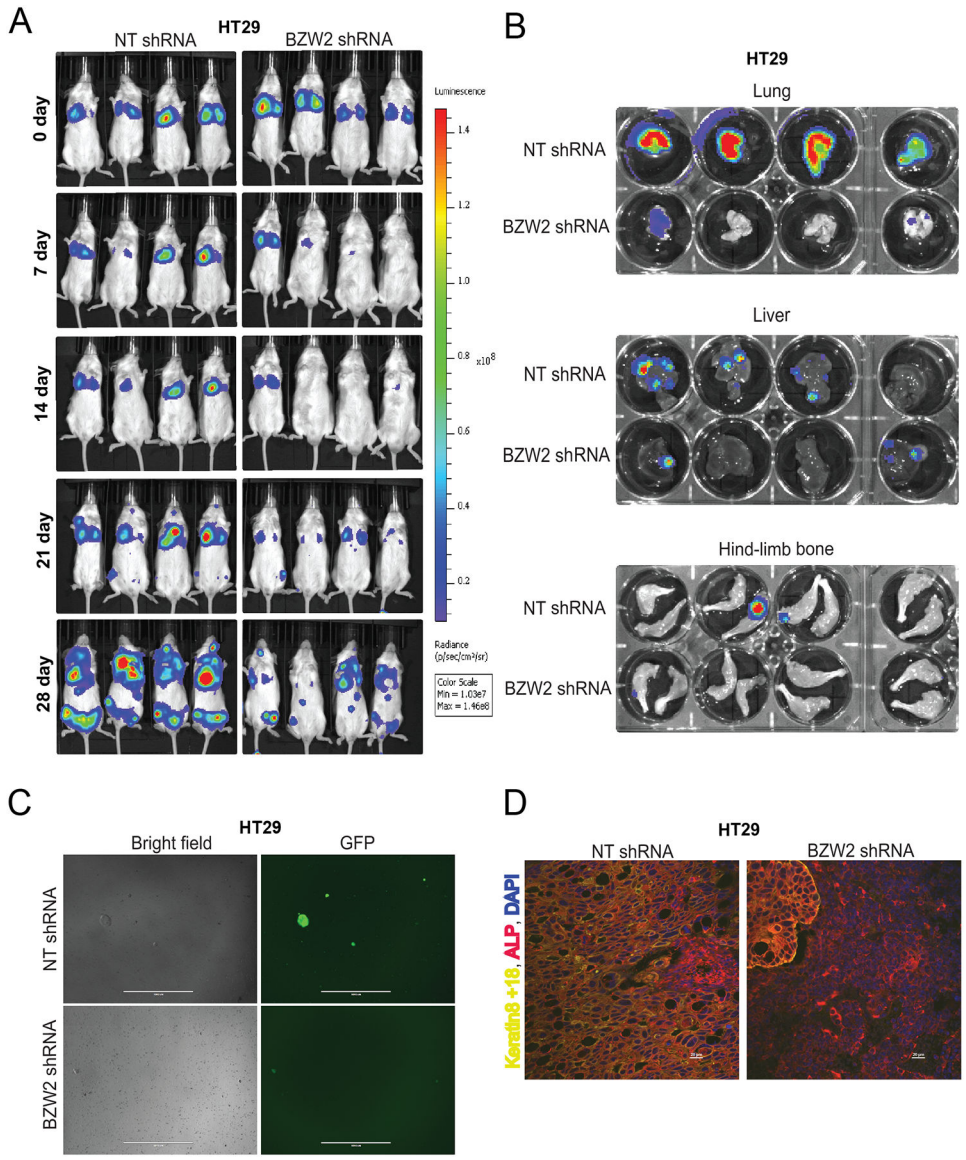

Figure 3.

BZW2 involvement in CRC metastasis in a tail-vein metastasis model. **A**, HT29 cells exhibiting BZW2 shRNA or NT shRNA were injected into tail veins of NSG mice, and bioluminescence imaging was performed weekly by injecting luciferin intraperitoneally. **B**, *Ex vivo* luminescence of organs procured after sacrifice of mice. **C**, Cultures of mouse bone marrow in media containing puromycin to select cancer cells. Representative phase-contrast and GFP images after 7 days showing cultured CRC cells from bone marrows of mice injected with HT29 cells exhibiting stably expressed NT shRNA or BZW2 shRNA (scale bar, 1000 μm. **D**, Keratin 8+18 (yellow) and ALP (red) co-staining of bone lesions of NT shRNA or BZW2 shRNA cells. DAPI was used for nuclear staining (scale bar, 20 μm).

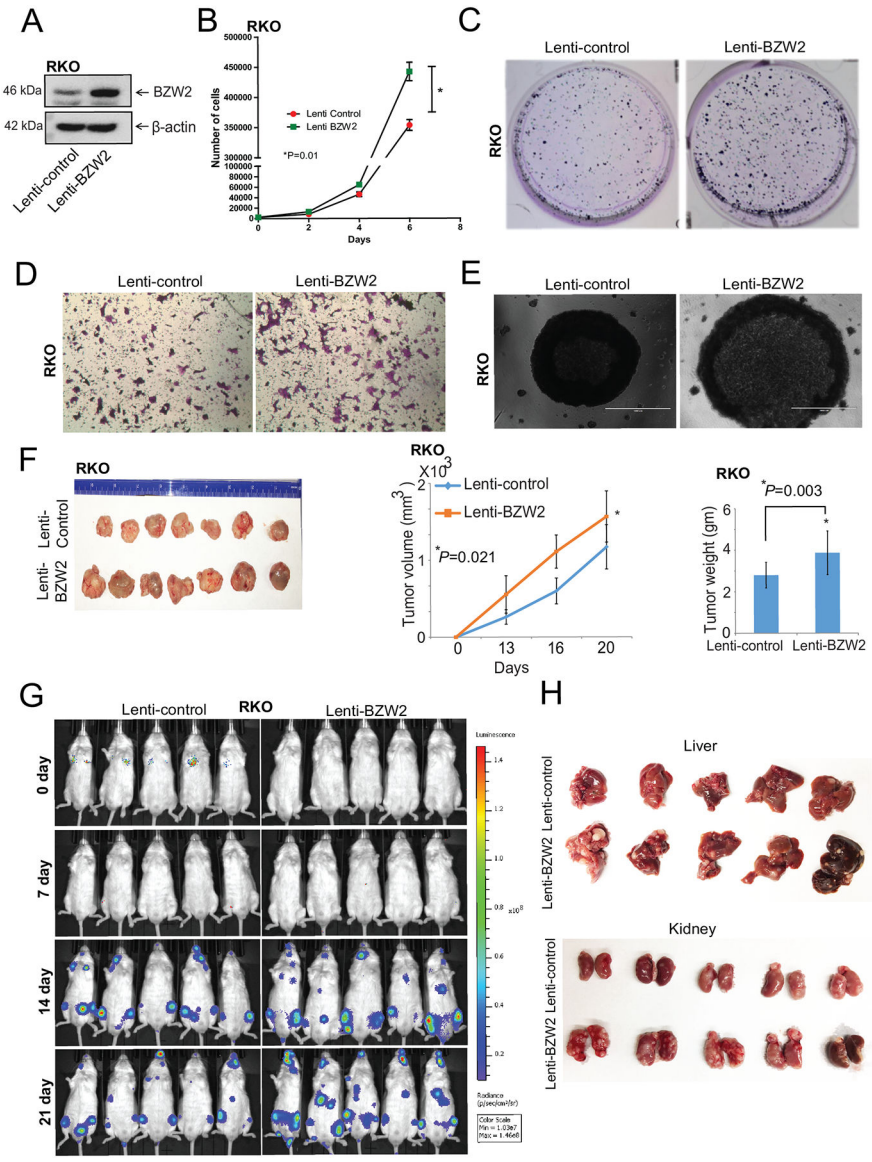

Figure 4.

Ectopic expression of BZW2 enhances malignant phenotypes of CRC. **A**, Expression of BZW2 in RKO cells was analyzed by Western blotting. **B**, Cell proliferation assay evaluating the effect of BZW2 overexpression on proliferation of RKO cells. **C**, Representative images of crystal violet-stained colonies of RKO cells transfected with a lenti-control or lenti-BZW2. **D**, Invasion capacity of BZW2-overexpressing or control vector RKO cells examined by a Transwell Matrigel invasion assay. **E**, Representative spheroids formed after BZW2 overexpression in RKO cells. **F**, BZW2 overexpressing or control vector RKO cells (2×10^6/mouse) were injected subcutaneously into NSG mice. On day 20, the six mice were sacrificed, and tumors were harvested. Values are presented as the means ± SD. **G**, *In vivo* luminescence imaging of NSG mice with RKO cells exhibiting BZW2 overexpression or control vector was performed. **H**, Representative photographs of liver and kidney retrieved from the metastasis experiment.

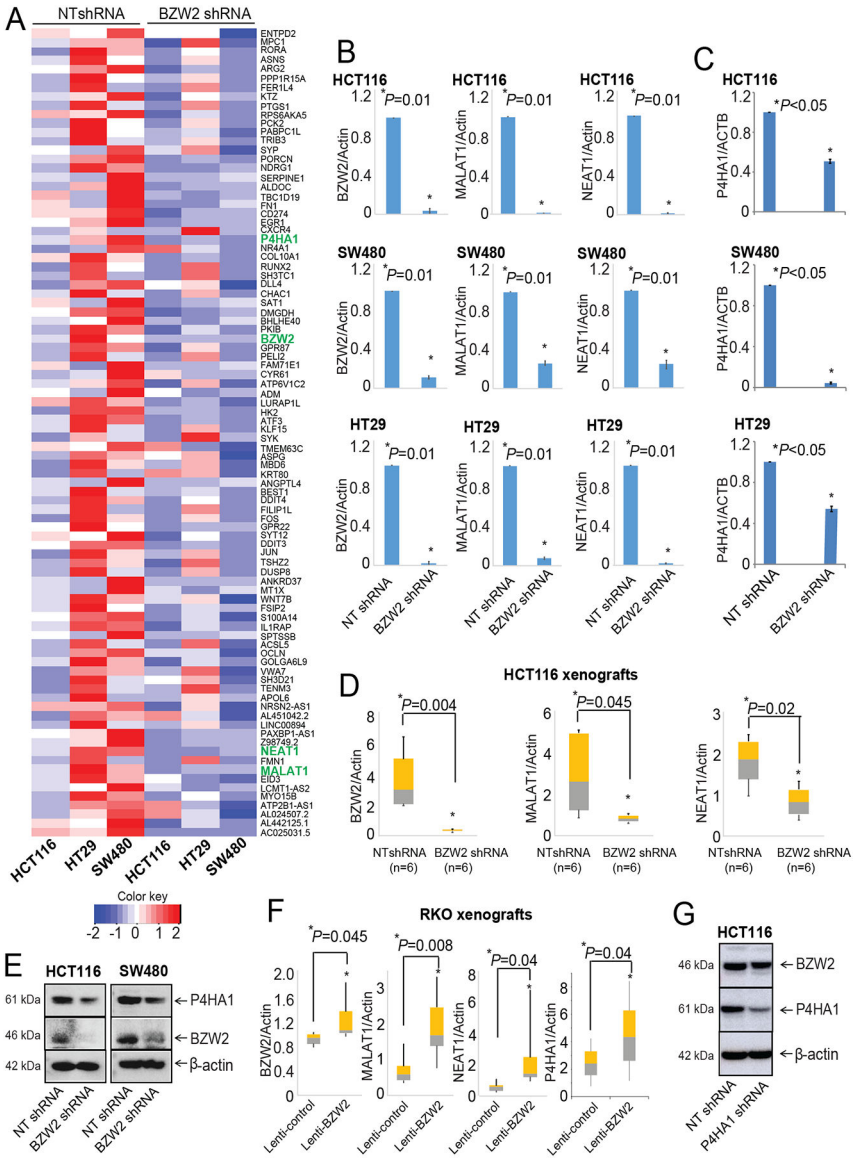

Figure 5.

MALAT1 and NEAT1 as downstream targets of BZW2 in CRC. **A**, Heatmap of differentially expressed genes from expression profiling of stable BZW2-knockdown HCT116, SW480, and HT29 cells. **B**, qRT PCR analysis of BZW2, MALAT1, and NEAT1 and **C**, P4HA1 in RNA of HCT116, SW480, and HT29 cells with stable BZW2-knockdown. **D**, RNA expression of BZW2, MALAT1, and NEAT1 in xenografts of HCT116 exhibiting BZW2 knockdown. **E**, Western blot analysis showing the expression of P4HA1 in BZW2-knockdown CRC cells. **F**, RNA expression of BZW2, MALAT1, NEAT1, and P4HA1 in BZW2-overexpressing RKO xenografts. Quantitative data are means ± SD. **P* < 0.01. **G**, The expression of BZW2 was measured after knockdown of P4HA1.

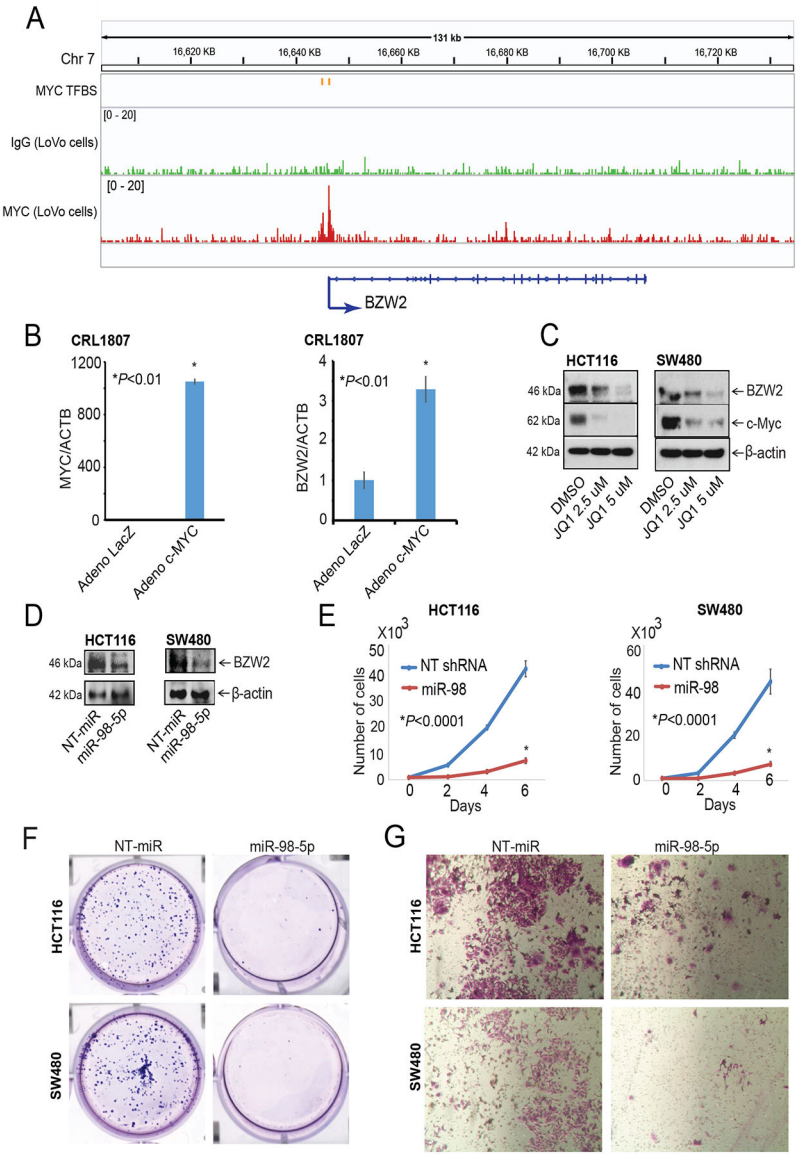

Figure 6.

BZW2 regulation by MYC and miR-98 in CRC. **A**, MYC transcription binding sites in the BZW2 promoter region: IGV snapshots of MYC ChIP-seq data [GSE51290] for gene and promoter region of BZW2. Top track shows MYC binding sites; the next two tracks indicate ChIP-seq read coverage on antibody treatment (MYC) and IgG in CRC cells (LoVo). LacZ control and MYC adenovirus were transduced into SV-40 transformed CRL1807 colon cells. **B** qRT-PCR analysis was performed to assess the RNA expression of MYC and BZW2 after MYC overexpression. **C**, HCT116, and SW480 cells were exposed to JQ1 followed by probing for BZW2 and c-Myc. **D**, HCT116, and SW480 cells were transfected with NT-pre-miR or miR-98. Immunoblot analyses were performed to assess BZW2 protein expression. Ectopic expression of NT-pre-miR or miR-98 was performed for HCT116, and SW480 cells to assess **E**, cell proliferation, **F**, colony formation, and **G**, invasion.

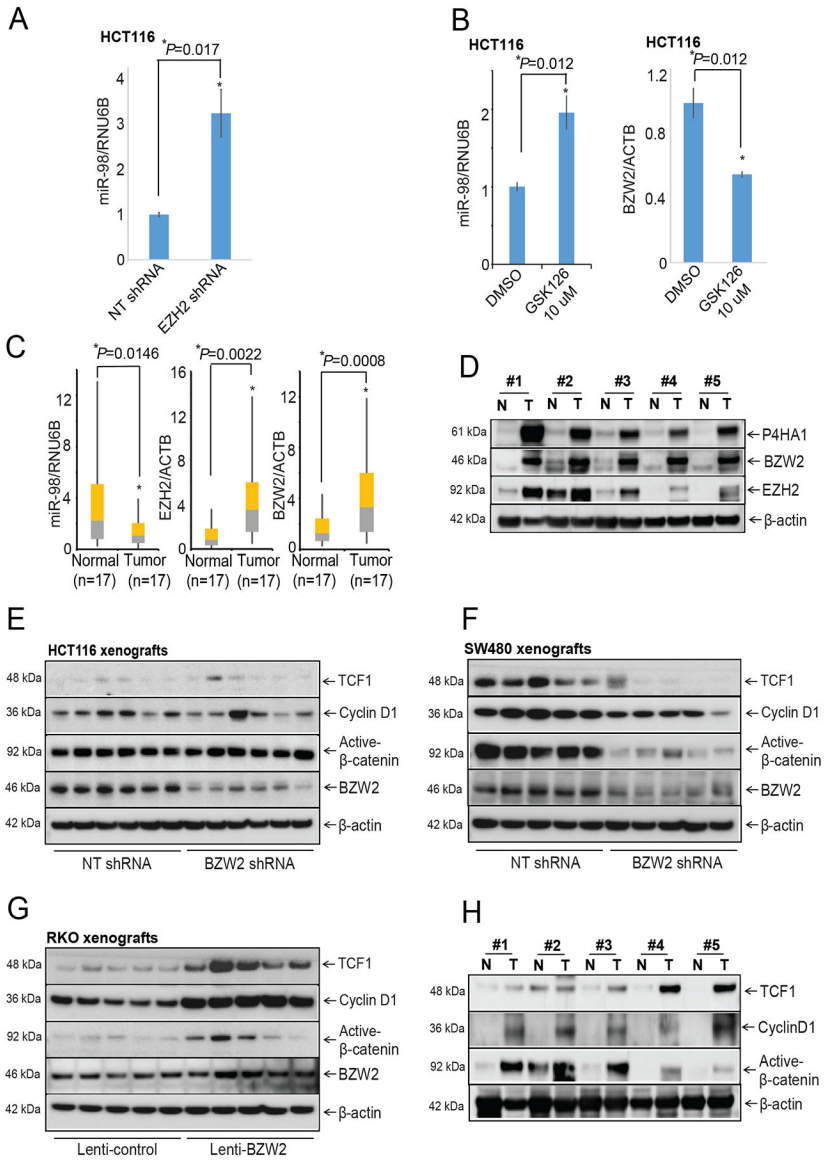

Figure 7.

EZH2 regulates BZW2, which activates the WNT/β-catenin signaling pathway in CRC. **A**, qRT-PCR analysis showing the expression of miR-98 and **B**, qRT-PCR analysis to assess the expressions of miR-98 and BZW2 in GSK-126-treated CRC cells. **C**, qRT-PCR analysis showing the relation of miR-98 with EZW2 or BZW2 in human CRC samples. **D**, Protein levels of EZH2, BZW2, and P4HA1 were measured in human CRCs (denoted by T) and matched adjacent normal breast (denoted by N) tissues (n = 5) by Western blot analysis. WNT/β-catenin signaling molecules, active-β-catenin, LEF1, and TCF1 protein levels were measured in xenografts of **E**, HCT116. **F**, SW480 and **G**, RKO having modulated BZW2 expression. **H**, Protein levels of WNT/β-catenin signaling molecules were measured in CRC (denoted by T) and matched adjacent normal (denoted by N) tissues (n = 5), that were used

in Fig 7D, by Western blot analysis. Quantitative data are presented in means ± SD. *$P <$ 0.01.